One New Super-Twisting Sliding Mode Direct Thrust Control for Linear Induction Machine Based on Linear Metro

Mosaad M. Ali, Wei Xu, *Senior Member, IEEE*, Abdul Khalique Junejo, Mahmoud F. Elmorshedy, *Member, IEEE*, and Yirong Tang, *Student Member, IEEE*

***Abstract*—In this article, a new supertwisting sliding mode direct thrust control (NSTSM-DTC) scheme is proposed to improve the dynamic response, robustness ability of the linear induction machine, and overall drive performance. First, a NSTSM algorithm is proposed and implemented in both electromagnetic thrust and primary flux-linkage control loops. The design aspects, implementation process, and stability analysis of the NSTSM based on the DTC method are fully investigated, which can effectively achieve faster dynamic response, smaller steady state speed tracking error, lower electromagnetic thrust ripple, and increase the system robustness against load variation in comparison to those of the conventional control methods. The proposed method is fully confirmed by the comprehensive simulations and experiments based on one prototype of 3 kW arc induction machine.**

***Index Terms*—Direct thrust control (DTC), end effects, linear induction machine (LIM), sliding mode control (SMC), supertwisting sliding mode (STSM).**

Manuscript received February 28, 2021; revised May 29, 2021; accepted July 3, 2021. Date of publication July 9, 2021; date of current version September 16, 2021. This work was supported in part by the National Natural Science Foundation of China under Grant 51877093, in part by the National Key Research and Development Program of China under Grant 2018YFE0100200, in part by the Key Technical Innovation Program of Hubei Province under Grant 2019AAA026, and in part by the fund from Science, Technology, and Innovation Commission of Shenzhen Municipality under Grant JCYJ20190809101205546. Recommended for publication by Associate Editor I. Slama-Belkhodja. *(Corresponding author: Wei Xu.)*

Mosaad M. Ali is with the State Key Laboratory of Advanced Electromagnetic Engineering and Technology, School of Electrical and Electronic Engineering, Huazhong University of Science and Technology, Wuhan 430074, China, and also with the Department of Electrical Engineering, Faculty of Engineering, Kafrelsheikh University, Kafr El-Shaikh 33516, Egypt. (e-mail: epe_mosaad@eng.kfs.edu.eg).

Wei Xu and Yirong Tang are with the State Key Laboratory of Advanced Electromagnetic Engineering and Technology, School of Electrical and Electronic Engineering, Huazhong University of Science and Technology, Wuhan 430074, China (e-mail: weixu@hust.edu.cn; yirtang@foxmail.com).

Abdul Khalique Junejo is with the State Key Laboratory of Advanced Electromagnetic Engineering and Technology, School of Electrical and Electronic Engineering, Huazhong University of Science and Technology, Wuhan 430074, China, and also with the Department of Electrical Engineering, Qaid-e-awam University of Engineering, Science and Technology, Nawabshah 67450, Pakistan (e-mail: ak.junejo@gmail.com).

Mahmoud F. Elmorshedy is with the Department of Electric Power and Machines Engineering, Faculty of Engineering, Tanta University, Tanta 31527, Egypt (e-mail: mahmoud.elmorshedy@f-eng.tanta.edu.eg).

Color versions of one or more figures in this article are available at https://doi.org/10.1109/TPEL.2021.3096066.

Digital Object Identifier 10.1109/TPEL.2021.3096066

Abbreviation List

LIM	Linear induction machine.
NSTSM-DTC	New super-twisting sliding mode direct thrust control.
NSTSM	New super-twisting sliding mode.
DTC	Direct thrust control.
AIM	Arc induction machine.
SMC	Sliding mode control.
STSM	Super twisting sliding mode.
RM	Rotary machine.
DTC-SVM	DTC with the space vector modulation scheme.
PI	Proportional-integral.
CSTSM	Conventional STSM.
CDTC	Conventional DTC.

I. Introduction

RECENTLY, linear induction machines (LIMs) have been widely used in modern industrial applications, especially for urban transportation drives [1]–[3]. This kind of application needs direct linear motion, strong acceleration/deceleration, low cost, minimum mechanical losses, and so on [4]. These industrial requirements can be achieved more easily by using the LIMs instead of the conventional rotary machines (RMs). Unfortunately, the control techniques for LIMs are more complicated than those of RMs due to stronger nonlinear traits and greater coupling relationship between primary and secondary mainly resulted from the end effects coming from open-magnetic circuit [5], [6], which would deteriorate the drive performance of the whole system as the speed goes up. Therefore, it is very necessary to develop one appropriate control strategy to strengthen the drive capability of the LIM and drive.

Direct thrust control (DTC) strategy has been paid a little attraction to the linear metro for its faster dynamic response, less dependency on machine parameters, stronger redundancy ability, simpler implementation, and so on [8]–[10]. Several modified schemes for the DTC methods have been introduced to achieve high dynamic performance for RMs in transient and steady-state operations [11]–[16]. Among these modifications, the use of DTC with the space vector modulation scheme (DTC-SVM) can overcome the variable switching frequency problem [11]. Comprehensive experiments have shown that the

DTC-SVM scheme can get better steady-state drive performance than other conventional DTC schemes in terms of the ripples of both primary flux and electromagnetic thrust [12]. Moreover, it is common to use a linear proportional-integral (PI) controller in the DTC-SVM method for the thrust and flux control loops. As it is known, the traditional PI controller has a poor behavior at load variations, especially for multi-variable nonlinear control systems [14]–[16]. Moreover, the thrust and flux-linkage ripples are still larger, and the dynamic characteristics of the control method are insufficient in this method. Hence, it is very necessary to put forward further improvements for the DTC-SVM to enhance the dynamic performance of the LIM drive system.

Thereof, one high performance LIM drive system can be achieved by using a robust controller instead of the PI controller. One of the potential techniques suitable to the transportation is the sliding mode control (SMC) due to its adaptability to load variations, robustness, insensitive to unknown parameter and disturbance, and easy implementation in practice. By comparing with the intelligent control techniques, such as fuzzy and neural network control techniques [17], [18], the SMC has been gradually used in some industrial applications, which can benefit from one better dynamic performance at the transient condition. Unfortunately, the SMC suffers one inherent chattering problem with high-frequency as produced by the controlled variables in different working states [19], [21].

Recently, the supertwisting sliding mode (STSM) controller has been developed for the RM drive system, which is totally different from the conventional SMC. In this condition, the STSM is working in high order sliding modes to eliminate the steady-state chattering and enhance the drive system performance. Moreover, the STSM control technique can enjoy merits of easy implementation, strong robustness, accurate operation, small control error of the first derivation, fast dynamic response, and so on [22]–[24]. In [25], the STSM algorithm is implemented for the current loops. In both [26] and [27], the STSM algorithm is implemented for the speed and flux control observers. These studies in [25]–[27] mostly focus on the STSM algorithm based on the field orientation control strategy. Fortunately, the STSM is an effective tool for controlling uncertain nonlinear systems, few studies have been conducted on the STSM control for LIMs and drives in the past research. Moreover, until now the STSM algorithm based on the DTC strategy (CSTSM-DTC) have not been fully introduced to LIMs and drives except for [28]. But, the original contribution of this study is employing the conventional STSM (CSTSM) control algorithm, as proposed by [29], in the torque and flux loops for induction motor without any modification. On the other hand, few studies have been done on the CSTSM algorithm to further improve the dynamic characteristic of the drive system. Therefore, it is very necessary to adopt the conventional STSM based on DTC strategy (CSTSM-DTC) to the LIM drive system, and then modify this control strategy to achieve fast dynamic response and low thrust chattering.

In order to improve the transient and steady-state operation of the LIM drive system, one DTC-SVM strategy based on new STSM (NSTSM) algorithm is proposed in this article, which can get faster speed response, lower thrust chattering, etc. The NSTSM is implemented for both thrust and flux control loops simultaneously. Moreover, by the development of one dynamic model considering the end effect, the NSTSM-DTC can reduce the vibrations and noise problems in the LIM drive system. The NSTSM algorithm can be achieved by adding one power exponential term ($|s|^{\alpha 2}$) in the dynamic equation of the CSTSM, which can help the system state reach the sliding mode surface much quicker with smoother steady-state operation. The NSTSM-DTC can effectively reduce the chattering phenomenon of the whole control system.

II. Preliminaries for the LIM Based On DTC-SVM Method

A. LIM Drive System Modeling

The LIM dynamic model based on the equivalent circuit introduced in [2], can be obtained with the help of the synchronous reference frame [30]. The LIM model can be described by the following equations. The dynamic voltages, flux-linkages and thrust equation can be described as follows:

The *dq*-axis voltages can be calculated by

$$u_{dq1} = R_1 i_{dq1} + p\psi_{dq1} - j\omega_1 \psi_{dq1} \tag{1}$$

$$u_{dq2} = R_2 i_{dq2} + p\psi_{dq2} - j\omega_{slip} \psi_{dq2} = 0 \tag{2}$$

where the primary and secondary variables are represented in the subscripts of 1 and 2, respectively. The *d*-axis and *q*-axis are referred to *dq*-axis of synchronous reference frame. Furthermore, *R* is the resistance, *u* the voltage, *i* the current and Ψ the flux-linkage of the LIM system, separately. Also, the slip speed is denoted as $\omega_{\text{slip}} = \omega_1 \text{-} \omega_2$, where ω_1 and ω_2 are the synchronous and the secondary speed.

The *dq*-axis linkage fluxes relationship can be written by

$$\psi_{dq1} = L_1 i_{dq1} + L_{meq} i_{dq1} \tag{3}$$

$$\psi_{dq2} = L_2 i_{dq2} + L_{meq} i_{dq2} \tag{4}$$

where L_1 is the primary inductance, L_2 the secondary inductance, and L_{meq} the effective magnetizing inductance.

The electromagnetic thrust can be determined by

$$F_e = (3\pi/2\tau)(\psi_{d1} i_{q1} - \psi_{q1} i_{d1}) \tag{5}$$

where τ is considered as the pole pitch. Meanwhile, by considering the attraction force and end-effect dynamics, the LIM parameters, such as mutual inductance and secondary resistance, would be modified by one coefficient, *f(Q),* as dependent on the end-effect factor *Q* as follows [2]:

$$f(Q) = (1 - \exp(-Q))/Q \tag{6}$$

$$Q = L_p R_2 / L_{b0} v_r \tag{7}$$

where L_p and L_{b0} are the primary length and the secondary inductance at standstill, respectively. The adapted mutual inductance can be described as

$$L_{m\text{eq}} = [1 - f(Q)] L_m \tag{8}$$

where L_m is the mutual inductance without end effect, similar as that of rotary induction machine [2], [30].

B. Primary Flux and Electromagnetic Thrust Dynamics

The DTC-SVM control method can be achieved through the primary flux-linkage orientation idea, where $\Psi_{d1} = \Psi_1$ and $\Psi_{q1} = 0$. According to this concept, the primary d-axis voltage equations can be revised as follows [10]–[12]:

$$u_{d1} = R_1 i_{d1} + p\psi_{d1}. \tag{9}$$

Also, the electromagnetic thrust equation can be expressed as

$$F_e = (3\pi/2\tau R_1)\psi_1(u_{q1} - \omega_1\psi_1). \tag{10}$$

It can be concluded from (9) and (10) that the value of primary flux-linkage can be controlled through the d-axis secondary voltage and the electromagnetic thrust can be adjusted by q-axis primary voltage, respectively.

III. Proposed Control Strategy for the LIM

In this section, the design procedure of the conventional and the new super-twisting SMC based on DTC-SVM for LIMs will be discussed in details as follows.

A. Design of the Conventional Supertwisting Sliding Mode Direct Thrust Control

In the CSTSM-DTC, the primary flux-linkage and thrust errors can be represented as the state-space of the LIM drive system, as illustrated by

$$\begin{cases} x = \begin{bmatrix} e_d & e_q \end{bmatrix}^T = \begin{bmatrix} |\psi_1{}^*| - |\psi_1| & F_e{}^* - F_e \end{bmatrix}^T \\ u = \begin{bmatrix} u_{d1} & u_{q1} \end{bmatrix}^T \end{cases} \tag{11}$$

where $\psi_1{}^*$ and $F_e{}^*$ are the references of the electromagnetic thrust and primary flux-linkage, respectively. The state variables e_d and e_q are the primary flux-linkage and thrust errors, respectively. Meanwhile, u is the output of the control method. The surface of the super twisting structure, s, is designed to equal the errors of flux and thrust, e_d and e_q, respectively, [27], [28]. The dynamic equations for the flux control loop based on the CSTSM algorithm can be described by

$$\begin{aligned} u_{d1} &= k_d |e_d|^r \operatorname{sgn}(e_d) + w_d \\ \dot{w}_d &= -\varepsilon_d \operatorname{sgn}(e_d) \end{aligned} \tag{12}$$

where k_d, ε_d, and r are the selected positive switching gains. The output variable of the CSTSM has a nonlinear continuous term, which is controlled by adjusting the exponent r, as recommended as 0.5 in this article [31].

Moreover, the dynamic error of the primary flux-linkage can be obtained by adopting the d-axis voltage, u_{d1}, as the control input for (9), as given by

$$\dot{e}_d = -k_d |e_d|^r \operatorname{sgn}(e_d) - w_d + R_1 i_{d1}. \tag{13}$$

It is seen that the CSTSM algorithm can be designed to make the variable states arrive at the sliding surface in a finite time. On the other hand, the additional feedforward term, $R_1 i_{d1}$, can be compensated by w_d effectively. Meanwhile, the CSTSM algorithm for the thrust control loop is described by the similar way as

$$\begin{aligned} u_{q1} &= k_q |e_q|^r \operatorname{sgn}(e_q) + w_q \\ \dot{w}_q &= \varepsilon_q \operatorname{sgn}(e_q) \end{aligned} \tag{14}$$

where $(\varepsilon_q \geq 0)$ and $(k_q > 0)$ are constant coefficient gains, which are both greater than zero.

For the desirable constant magnitude of the primary flux, the thrust dynamic error can be obtained by evaluating the derivation of (10), as given by

$$\dot{e}_q = \kappa \dot{i}_{q1} = -N k_q |e_q|^r \operatorname{sgn}(e_q) - N w_q + E \tag{15}$$

where $\kappa = 3\pi\psi_{d1}/2\tau$, $N = 3\pi\psi_1/2\tau L_1\sigma$, and E is one disturbance. According to the theory of SMC, w_q would become equivalent to E in a finite time. The flux and thrust control strategies based on CSTSM are designed to adjust the d- and the q-axis voltages simultaneously. In this way, the output of the CSTSM-DTC can be obtained by

$$\begin{bmatrix} u^*{}_{d1} \\ u^*{}_{q1} \end{bmatrix} = \begin{bmatrix} k_d |e_d|^r \operatorname{sgn}(e_d) + \int \varepsilon_d \operatorname{sgn}(e_d) \\ k_q |e_q|^r \operatorname{sgn}(e_q) + \int \varepsilon_q \operatorname{sgn}(e_q) \end{bmatrix}. \tag{16}$$

The schematic illustration of the CSTSM for both flux and thrust control loops is shown in Fig. 1.

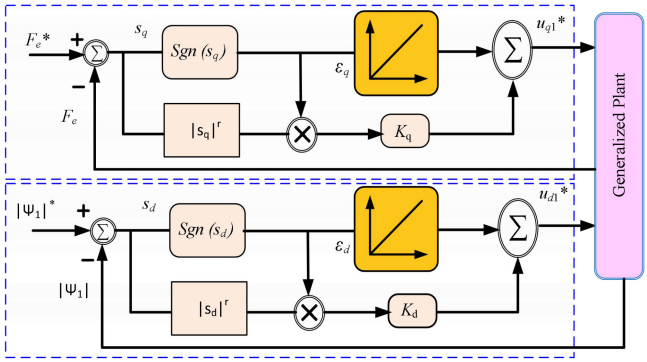

Fig. 1. Schematic illustration of the CSTSM-DTC for thrust and primary flux control loops.

B. Design of the New Supertwisting Sliding Mode Direct Thrust Control

The CSTSM reachability condition ensures that the moving point at any position in the state-space can reach the switching surface within a limited time, and there is no restriction on the motion trajectory. Moreover, the CSTSM control output law plays the main role of improving the dynamic quality of the reaching movement. Therefore, a new STSM control output law is designed in such a way to improve the dynamic response of the system and reduce the chattering phenomena effectively by adding a second exponent power term. It can be described as

$$\begin{aligned} u &= -k_p |s|^{\alpha 1} \operatorname{sgn}(s) - k_i |s|^{\alpha 2} + w_d \\ \dot{w}_d &= \varepsilon \operatorname{sgn}(s) \end{aligned} \tag{17}$$

where s is the system surface, k_p and k_i are constant positive gains, and α_1 and α_2 the exponent gains with a small positive

value less than one. The second exponent power term, $k_i|s|^{\alpha 2}$, plays a leading role in both transient and steady state operation.

This NSTSM algorithm makes the system states reach faster the sliding surface and achieve smoother transition to the sliding surface, which can dramatically weaken the system chattering phenomenon. More information can be found below.

The Primary Flux and electromagnetic thrust control loops based on the NSTSM algorithm are described by

$$u = \begin{bmatrix} u_{d1} \\ u_{q1} \end{bmatrix} = \begin{bmatrix} k_{pd}|e_d|^{\alpha 1}\mathrm{sgn}(e_d) + k_{id}|e_d|^{\alpha 2} - w_{dn} \\ k_{pq}|e_d|^{\alpha 1}\mathrm{sgn}(e_q) + k_{iq}|e_d|^{\alpha 2} - w_{qn} \end{bmatrix}. \tag{18}$$

The parameters k_p, k_i and ε_p are positive and constant to be selected for both thrust and flux loops. The second terms, w_{dn} and w_{qn}, appear as perturbations in (18), as described by

$$\begin{bmatrix} \dot{w}_{dn} \\ \dot{w}_{qn} \end{bmatrix} = \begin{bmatrix} -\varepsilon_{pd}\mathrm{sgn}(e_d) \\ -\varepsilon_{pq}\mathrm{sgn}(e_q) \end{bmatrix}. \tag{19}$$

So, the first derivative of the sliding surface for the electromagnetic thrust and primary flux-linkage control loops are described by

$$\begin{aligned} \dot{s}_d &= -k_{pd}|e_d|^{\alpha 1}\mathrm{sgn}(e_d) - k_{id}|e_d|^{\alpha 2} - w_{dn} + R_1 i_{d1} \\ \dot{s}_q &= -k_{pq}|e_d|^{\alpha 1}\mathrm{sgn}(e_q) - k_{iq}|e_d|^{\alpha 2} - w_{qn} + E. \end{aligned} \tag{20}$$

Hence, the novel STSM controller based on the two exponent power terms is proposed for the thrust and primary flux control loops in this article, as given by

$$\begin{bmatrix} u_{d1} \\ u_{q1} \end{bmatrix} = \begin{bmatrix} k_{pd}|e_d|^{\alpha 1}\mathrm{sgn}(e_d) + k_{id}|e_d|^{\alpha 2} + \int \varepsilon_d \mathrm{sgn}(e_d) \\ k_{pq}|e_q|^{\alpha 1}\mathrm{sgn}(e_q) + k_{iq}|e_q|^{\alpha 2} + \int \varepsilon_q \mathrm{sgn}(e_q) \end{bmatrix}. \tag{21}$$

Due to the serious chattering phenomenon of the discontinuous sign function, sgn(s), the boundary layer method is used instead of the sgn function because it depends mostly on the continuous saturation function, as defined by

$$\mathrm{sgn}(s_y) = \begin{cases} 1 if (s_y > \gamma) \\ s_y/\gamma if (|s_y| \le \gamma) \\ -1 if (s_y < -\gamma) \end{cases} \tag{22}$$

where γ is a small value and the subscript y denoted to the d- or q-axis error, the primary flux-linkage or electromagnetic thrust error, respectively. For further improvement, the function sgn(s_y) can be expressed by

$$\mathrm{sat}(s_y) = \frac{s_y}{s_y + \gamma}. \tag{23}$$

Finally, the control law of the NSTSM-DTC can be further modified as

$$\begin{bmatrix} u^*_{da} \\ u^*_{qa} \end{bmatrix} = \begin{bmatrix} k_{pd}|e_d|^{\alpha 1}\mathrm{sat}(e_d) + k_{id}|e_d|^{\alpha 2} + \int \varepsilon_d \mathrm{sat}(e_d) \\ k_{pq}|e_q|^{\alpha 1}\mathrm{sat}(e_q) + k_{iq}|e_q|^{\alpha 2} + \int \varepsilon_q \mathrm{sat}(e_q) \end{bmatrix}. \tag{24}$$

The schematic illustration of the proposed NSTSM for thrust and primary flux control loops according to (24) is illustrated in Fig. 2. The block diagram of the LIM drive system based on the NSTSM-DTC strategy is illustrated in Fig. 3. As seen from Figs. 2 and 3, the PI controller uses the linear speed error to obtain the dynamic electromagnetic thrust reference. The actual

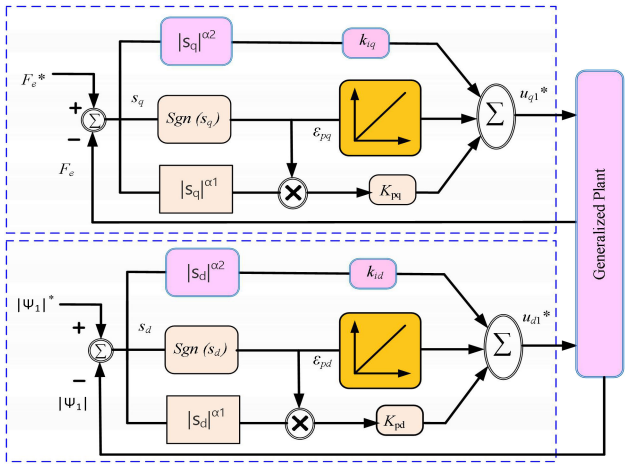

Fig. 2. Schematic illustration of the NSTSM-DTC for thrust and primary flux control loops.

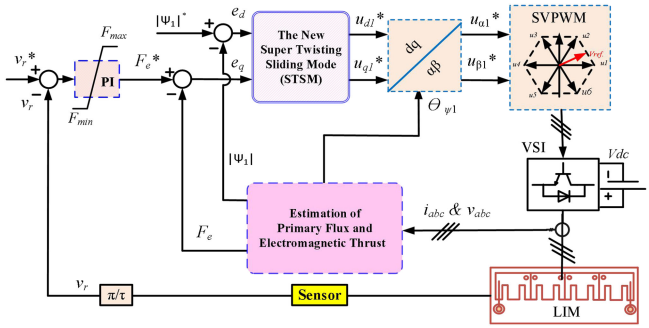

Fig. 3. Block diagram of the NSTSM-DTC for the LIM drive system.

electromagnetic thrust is calculated by (5) and the primary flux-linkage can be estimated by the voltage model equation using the discrete simulation technique, as given by

$$\left.\begin{aligned} u^*_{\alpha 1} &= R_1 i_{\alpha 1} + \frac{\psi^*_{\alpha 1} - \psi_{\alpha 1}}{T_s} \\ u^*_{\beta 1} &= R_1 i_{\beta 1} + \frac{\psi^*_{\beta 1} - \psi_{\beta 1}}{T_s} \end{aligned}\right\} \psi^*_1 = \sqrt{\left(\psi^*_{\alpha 1}\right)^2 + \left(\psi^*_{\beta 1}\right)^2} \tag{25}$$

where T_s is the sample time. Moreover, the thrust and primary flux errors are executed by the NSTSM controller to generate the reference dq-axis primary voltages. These reference values are converted to the $\alpha\beta$-axis coordinates using the primary flux angle. Finally, the $\alpha\beta$-voltage vectors ($u_{\alpha 1}{}^*$ and $u_{\beta 1}{}^*$) are handled by the space vector pulse width modulation technique to get the switching states for the voltage source inverter.

C. Stability Analysis

To check the proposed control methods, the stability condition based on Lyapunov theorem is proven as follows. For the electromagnetic thrust loop, it can get

$$v(x) = \frac{1}{2}s^2$$

$$\begin{aligned} v^{\bullet}{}_1 &= s_d * \dot{s}_d \\ &= s_d(-k_{pd}|s_d|^{\alpha 1}\mathrm{sgn}(s_d) - k_{id}|s_d|^{\alpha 2} - w_{dn} + R_1 i_{d1}) \end{aligned}$$

TABLE I
MAIN PARAMETERS OF THE PROPOSED NSTSM-DTC AND THE CSTSM FOR BOTH THRUST AND FLUX CONTROL LOOPS

Thrust		Flux	
Parameters	Values	Parameters	Values
k_{pq}= k_{iq}	5	k_{pd} = k_{id}	50
ε_q	1000	ε_d	5000
r	0.5	r	0.5
α_1, α_2, γ	0.5, 1.3, 0.02	α_1, α_2, γ	0.5, 1.3, 0.02

TABLE II
MAIN PARAMETERS OF THE LIM

Symbol	Quantity	Value	Unit
v_N	Nominal speed	11	m/s
F_N	Nominal thrust	270	N
I_N	Nominal current	22	A
τ	Pole pitch	0.1485	m
l_s	Primary length	1.3087	m
L_{la}	Primary leakage inductance	0.0114	H
R_b	Secondary resistance	2.4	Ω
R_a	Primary resistance	1.2	Ω

$$= s_d(-k_{pd}|s_d|^{\alpha 1}\mathrm{sgn}(e_d) - k_{id}|s_d|^{\alpha 2} - w_{dn} + R_1 i_{d1})$$
$$= s_d(-k_{pd}|s_d|^{\alpha 1}\mathrm{sgn}(e_d) - k_{id}|s_d|^{\alpha 2} - \varepsilon_d \int \mathrm{sgn}(s_d) + R_1 i_{d1})$$
$$= -k_{pd}|s_d|^{\alpha 1+1} - k_{id}|s_d|^{\alpha 2+1} - \varepsilon_d \zeta_d + R_1 i_{d1} \le 0. \quad (26)$$

For a large enough ε_d, the above inequality condition can be satisfied easily. For the primary flux-linkage loop, it can get

$$v^{\bullet}{}_2 = s_q * \dot{s}_q$$
$$= s_q(-k_{pq}|e_d|^{\alpha 1}\mathrm{sgn}(e_q) - k_{iq}|e_d|^{\alpha 2} - w_{qn} + E)$$
$$= s_q(-k_{pq}|e_d|^{\alpha 1}\mathrm{sgn}(e_q) - k_{iq}|e_d|^{\alpha 2} - \varepsilon_q \int \mathrm{sgn}(s_q) + E)$$
$$= -k_{pq}|s_q|^{\alpha 1+1} - k_{iq}|s_q|^{\alpha 2+1} - \varepsilon_q \zeta_q + E \le 0. \quad (27)$$

According to the Lyapunov theorem, the reaching condition ($s^*\dot{s}<0$) can be satisfied for both thrust and primary flux loops. It can guarantee that the NSTSM-DTC strategy is stable, and the sliding mode trajectory will reach zero in a finite time.

IV. SIMULATION AND EXPERIMENTAL VALIDATIONS

In order to investigate the advantages of the NSTSM-DTC method, comprehensive simulation and experiments have been made based on one prototype of the LIM with 3 kW rated power. The LIM drive system is simulated considering the end effect. The results based on the NSTSM-DTC are compared with those obtained under both CSTSM-DTC and CDTC strategies. The optimized control parameters of the NSTSM-DTC and the CSTSM-DTC control methods are given in Table I, which are used for both simulation and experiments. Main parameters of the employed LIM are given in Table II.

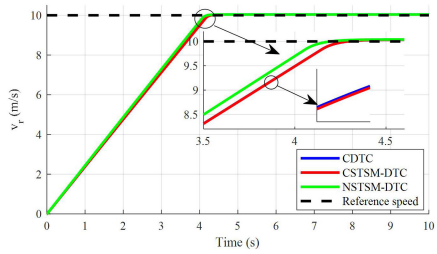

Fig. 4. Speed responses of the LIM under the CDTC, CSTSM-DTC, and NSTSM-DTC strategies.

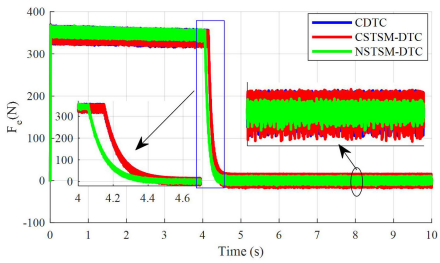

Fig. 5. Corresponding LIM electromagnetic thrust during the starting up operation.

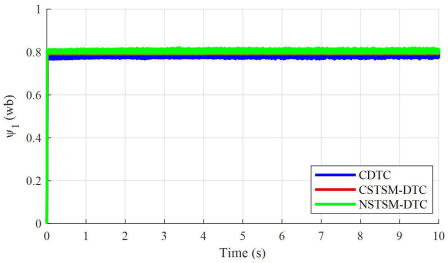

Fig. 6. Primary flux of LIM during the starting up process.

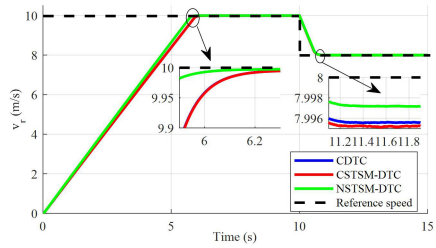

Fig. 7. Linear speed profile for the three control methods.

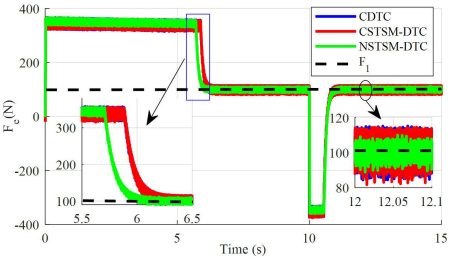

Fig. 8. Corresponding electromagnetic thrust response for the three control methods under sudden linear speed change.

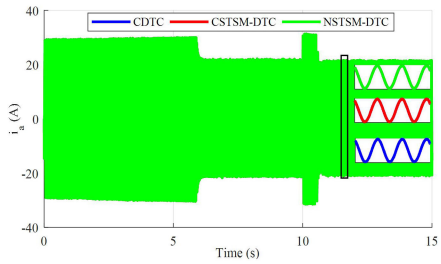

Fig. 9. Input Phase-A response for the three control methods under sudden linear speed change.

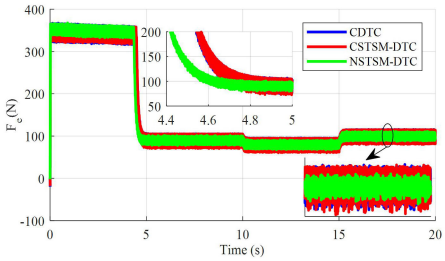

Fig. 10. Behavior of electromagnetic thrust.

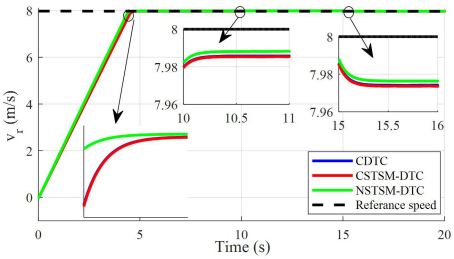

Fig. 11. Linear speed responses under thrust load variation for the three control strategies.

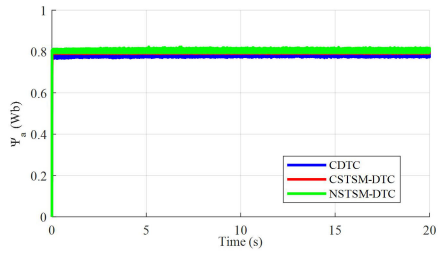

Fig. 12. Response of the primary flux-linkage under thrust load variation for the three control strategies.

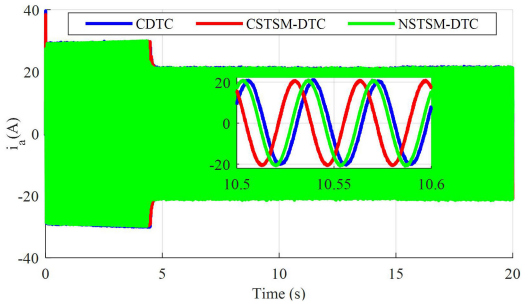

Fig. 13. Input Phase-A current response under thrust load variation based on the three control strategies.

TABLE III
COMPARISON OF THE TRANSIENT AND STEADY-STATE PERFORMANCE AMONG CDTC, CSTSM-DTC, AND NSTSM-DTC STRATEGIES

Quantity	CDTC	CSTSM-DTC	NSTSM-DTC
Settling time at start-up operation without load (0 m/s to 10 m/s)	4.3 s	4.3 s	4.15 s
Settling time at start-up operation with load of 100N (0 m/s to 10 m/s)	6.35 s	6.34 s	6.1 s
Steady-state speed error at speed decrease (10 m/s to 8 m/s)	0.0048	0.0044	0.0028
Steady-state error at Load increase (100 N to 75 N)	0.026	0.0265	0.0235
Thrust ripple percentage at steady-state performance	15%	15%	8%

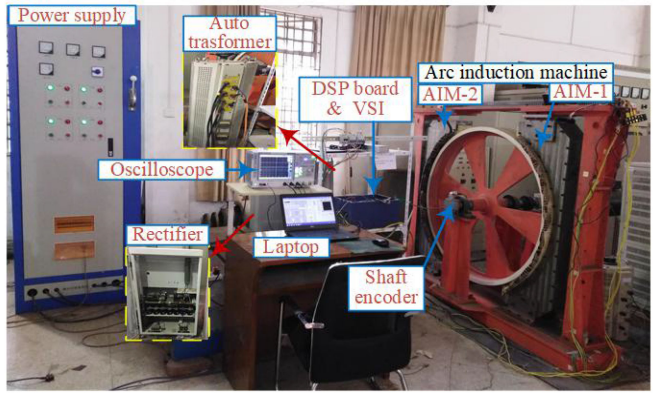

Fig. 14. Experimental platform of the AIM drive system.

A. Simulation Results

In this section, the LIM performance is analyzed under the NSTSM-DTC, CSTSM-DTC, and CDTC strategies with three different operating conditions. In order to obtain a fair comparison, the three control strategies have been done under the same thrust limitation and the same gain parameters of the speed control loop. Meanwhile, the control parameters for thrust and flux control loops are same in both NSTSM-DTC and CSTSM-DTC methods.

Case 1 Starting up Process: In this studying case, the system performance is tested under no load. Simultaneously, the linear speed is changed from standstill (0 m/s) to 10 m/s. The speed responses of the LIM under CDTC, CSTSM-DTC, and NSTSM-DTC strategies are depicted in Fig. 4. It is observed from this picture that the actual speed response under the proposed NSTSM-DTC can follow the desired speed very well in term of the quickest response, which confirms the effectiveness of the NSTSM algorithm. The corresponding LIM electromagnetic thrust is shown in Fig. 5. It can be noticed from this figure that the thrust response under the proposed NSTSM-DTC can settle to the steady-state in smaller time than those of CDTC and CSTSM-DTC, separately.

Moreover, Fig. 5 clearly shows that the ripples of the LIM electromagnetic thrust under the proposed NSTSM-DTC are

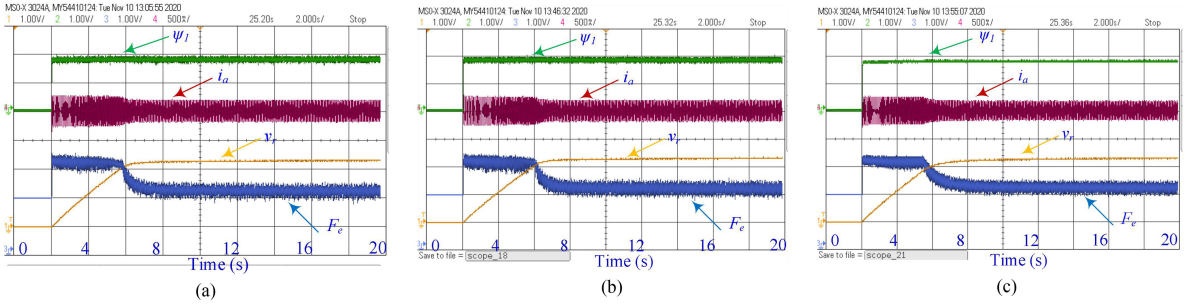

Fig. 15. Starting-up drive performance from 0 to 5 m/s for linear speed, electromagnetic thrust, input phase-A current, and primary flux-linkage. (a) New supertwisting sliding mode direct thrust control. (b) Conventional supertwisting sliding mode direct thrust control. (c) Conventional DTC.

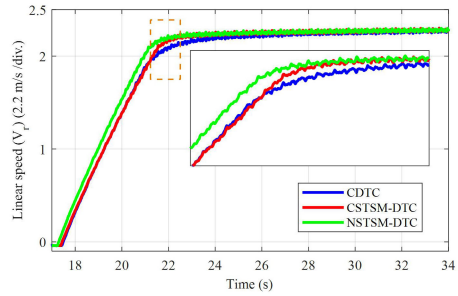

Fig. 16. Comparison of the AIM speed responses for the three control strategies.

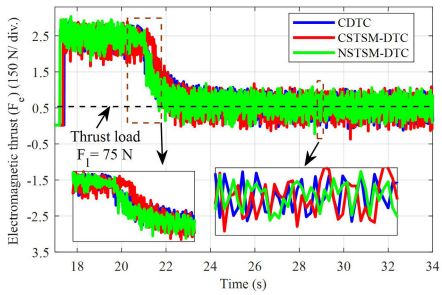

Fig. 17. Comparison of thrust responses for three control strategies under starting up.

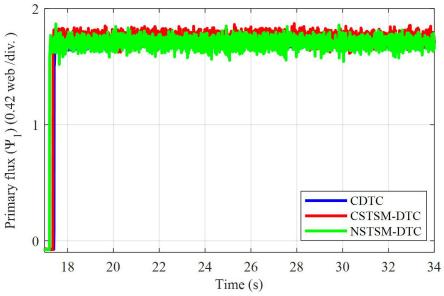

Fig. 18. AIM estimated primary flux-linkages for the three control strategies under starting up.

smaller than those obtained from CDTC and CSTSM-DTC methods. In addition, the resulting primary flux-linkage of the LIM is constant during the starting up process, as illustrated in Fig. 6.

Case 2 Variable LIM Speed Under Constant Thrust: The drive performance of the LIM system controlled by the CDTC, CSTSM-DTC, and NSTSM-DTC strategies is fully observed under a sudden linear speed change with a constant load. The LIM speed profile is presented in Fig. 7, where the desired linear speed is decreased from 10 to 8 m/s at t = 10 s.

Meanwhile, the load is maintained constant at 60 N. It is noted from the Fig. 7 that the speed response under the proposed control strategy, NSTSM-DTC, takes smaller settling time to reach the desired linear speed and smaller speed tracking error compared with the other two control methods, CDTC and CSTSM-DTC. The corresponding electromagnetic thrust responses of CDTC, CSTSM-DTC, and NSTSM-DTC under the sudden linear speed change are shown in Fig. 8. It can be observed that the speed change of LIM is directly proportional to the electromagnetic thrust that help to track the actual reference speed gradually. Also, from this picture, it can be observed that the thrust ripple based on the NSTSM-DTC strategy has lower value. On the other hand, the corresponding input phase-A current during speed changes is shown in Fig. 9. It is seen that the input Phase-A current changes directly with the variable linear speed, which similarly happens in the three controlled strategies aforementioned.

Case 3 Thrust-Load Change at Constant Speed: In this test, the NSTSM-DTC strategy is verified under a constant linear speed and variable thrust load. The linear speed is fixed at 8 m/s, while the load is decreased from 100 to 75 N at t = 10 s, and after 5 s it is increased again to 100 N. The behavior of electromagnetic thrust during three different loading levels based on the three control strategies are depicted in Fig. 10. As seen from this figure, the NSTSM-DTC can get the fastest dynamic response with smallest thrust ripple among the three algorithms.

Moreover, the linear speed responses under CDTC, CSTSM-DTC, and NSTSM-DTC strategies are depicted in Fig. 11, respectively. It can be seen that the actual linear speed can quickly follow the desired value with small steady state error, which ensures the effectiveness of the proposed NSTSM-DTC strategy. Fig. 12 describes the performance of primary flux-linkage, which is constant under load change for the CDTC, CSTSM-DTC and the NSTSM-DTC, individually. Finally, the LIM input phase-A current under different control strategies is shown in Fig. 13. It is seen that the input current response

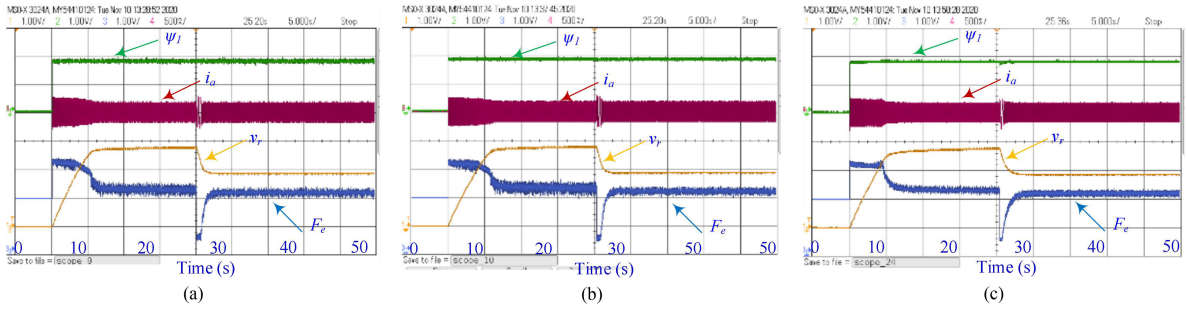

Fig. 19. Responses of speed variation under constant load for linear speed, electromagnetic thrust, input phase-A current, and primary flux-linkage. (a) New supertwisting sliding mode direct thrust control. (b) Conventional supertwisting sliding mode direct thrust control. (c) Conventional DTC.

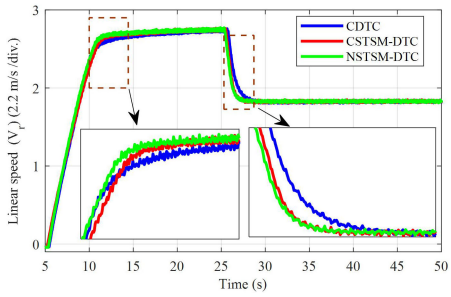

Fig. 20. Comparison of the AIM speed response for the three control strategies under the speed variation.

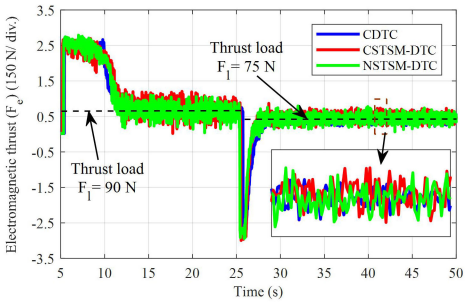

Fig. 21. Comparison of the thrust response for the three control strategies under the speed variation.

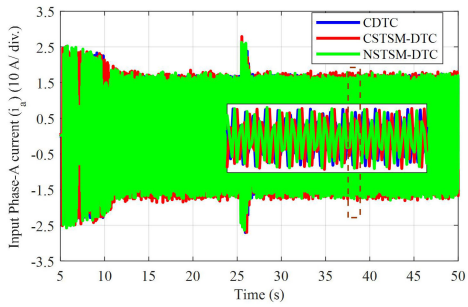

Fig. 22. AIM input Phase-A current based on the three control strategies under the speed variation.

can be modified in the same way as the load change by the three control methods. According to the simulation results, the comparison of the LIM performance under the three control strategies for different operating conditions is given in Table III. It is clear from Table III, that the NSTS-DTC strategy has the smallest settling time of linear speed response during the start-up operation compared to CSTSM-DTC and CDTC. Also, the proposed control strategy has the smallest steady-state speed error during load and speed variation as given in Table III. Moreover, the NSTSM-DTC strategy can reduce the steady-state ripple in electromagnetic thrust under different operating conditions compared to the other two control strategies. It is difficult to get accurate information, how much percentage improvement on the dynamic response and the steady-state tracking error, which varies with the operation states, such as the reference speed and the loading requirement, as illustrated in Table III. Meanwhile, the NSTSM-DTC strategy can reduce the steady-state ripple in electromagnetic thrust under different operating conditions by 7% compared to the other two control strategies.

B. *Experiments and Analysis*

For experimental verifications, one prototype, arc induction motor (AIM) with large radius, is built up to simulate the drive performance of practical LIM, as illustrated in Fig. 14. An incremental encoder and a hall current sensor are used to measure the rotating speed and the primary current, respectively. For the large radius, the circular movement can be approximated as linear movement. The load is managed by a permanent magnet synchronous generator coupled to the shaft of AIM, whose terminal is connected with three-phase variable resistance. The proposed NSTSM-DTC strategy executed in this prototype is fully compared with those of CSTSM-DTC and CDTC, respectively. The parameters of the employed AIM are listed in Table II. For a fair comparison, the thrust limitation and the speed gains are kept the same in all control methods.

In order to keep the safe operation, the dc voltage is limited to 340 V, and the maximum speed is about 6 m/s. Full investigations are made on the NSTSM-DTC strategy in three operating conditions, including starting up, speed variation under constant thrust load, and thrust load variation under constant speed. More details are given out as follows.

Case 1: Starting up Process: The starting up performance of the AIM is examined for the three control methods, where the speed is changed from 0 to 5 m/s with a light load representing the coupling and shaft losses. The dynamic responses of the

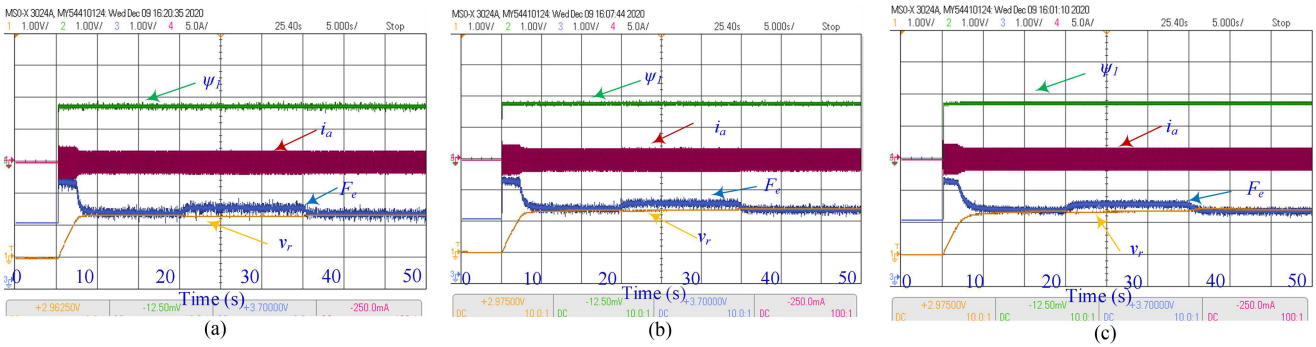

Fig. 23. Load variation responses for linear speed, electromagnetic thrust, input phase-A current, and primary flux-linkage. (a) New supertwisting sliding mode direct thrust control. (b) Conventional supertwisting sliding mode direct thrust control. (c) Conventional DTC.

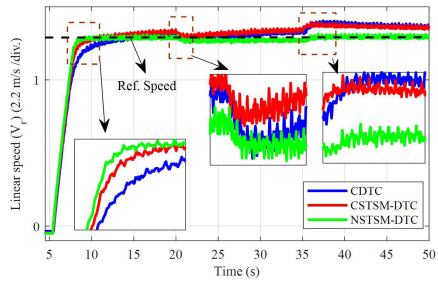

Fig. 24. Comparison of the AIM speed responses for three control strategies under thrust load variations.

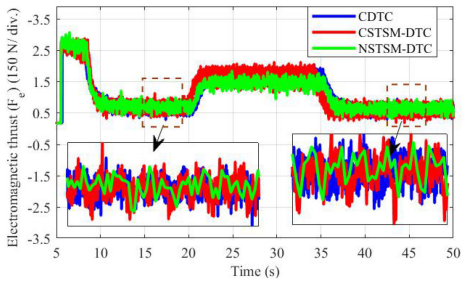

Fig. 25. Comparison of the thrust response of the three control strategies under the thrust variations.

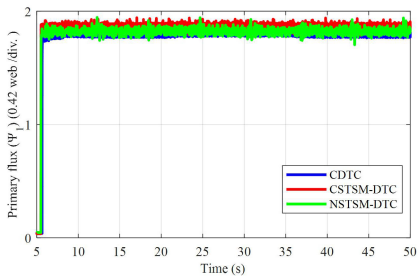

Fig. 26. AIM estimated primary flux linkage for three control strategies under thrust variations.

linear speed, electromagnetic thrust, input phase-A current, and primary flux-linkage for the NSTSM-DTC, CSTSMC-DTC, and CDTC methods during the starting up process are shown in Fig. 15(a)–(c), respectively. To illustrate the advantages of the

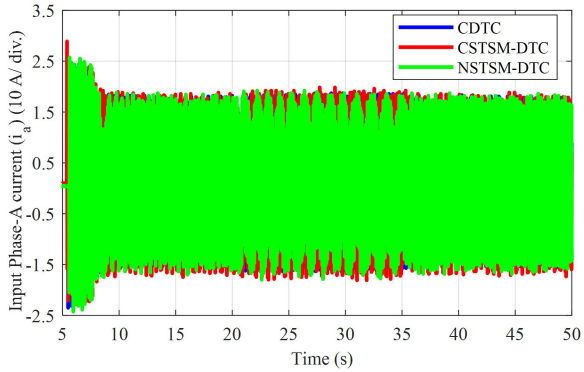

Fig. 27. AIM input Phase-A current for the three control strategies under the thrust load variations.

NSTSM-DTC over the other two control methods, the linear speeds of the three control methods are given out in Fig. 16. The AIM speed response during the starting up based on the NSTSM-DTC has faster response in comparison to the other two control methods. In the similar way, the electromagnetic thrust responses for the three control strategies are illustrated in Fig. 17. This figure proves that the thrust ripple of the proposed strategy, NSTSM-DTC, has the smallest value. Furthermore, Fig. 18 shows the estimated primary flux-linkages of the CDTC, CSTSM-DTC and NSTSM-DTC, which is almost constant under the three different algorithms.

Case 2: Variable Speed Under Constant Thrust Load: This test is presented to check the capability of the NSTSM-DTC over the other two control methods under variable linear speed and constant thrust load. The speed changes from standstill to 6 m/s during the first 20 s, and then the AIM speed decreases to 4 m/s while the thrust load is kept constant. The dynamic responses of the linear speed, electromagnetic thrust, input Phase-A current, and primary flux-linkage for the NSTSM-DTC, CSTSMC-DTC, and CDTC during the speed variation are shown in Fig. 19(a)–(c), respectively. Comparison of the AIM speed responses for the three control strategies are shown in Fig. 20. It is known that the AIM speed response under the NSTSM-DTC has the fastest response among these three methods. Also, the electromagnetic thrust response under the proposed method has the smallest ripple as illustrated in Fig. 21. Briefly, a small effect on the

thrust load happens due to the changing effect of the AIM speed in response to the rotating permanent magnet synchronous generator. Furthermore, the AIM input phase-A currents based on the three methods are altered due to the speed variation, as illustrated in Fig. 22.

Case 3: Variable Thrust Load Under Constant Speed: This testing is proposed to investigate the validity of the NSTSM-DTC under load variation condition. In general, the load changes from 80 to 225 N firsty, and after 15 s, the load decreases again to 80 N at constant speed of 3 m/s. Fig. 23(a)–(c) illustrates the dynamic responses of the linear speed, electromagnetic thrust, input phase-A current, and primary flux-linkage for the NSTSM-DTC, CSTSMC-DTC, and CDTC during the load variation. Comparison of the AIM speed responses for three control strategies under thrust load variations is shown in Fig. 24. As seen from this picture, the speed response of the proposed method has the smallest speed drop and speed overshoot during the load increase and decrease. In addition, the speed response under the NSTSM-DTC strategy has the fastest response approaching to the reference speed. Moreover, the electromagnetic thrust responses for the three-control strategies are illustrated in Fig. 25. As seen from this picture, the electromagnetic thrust response under the proposed method has the smallest value among the three methods. The estimated primary flux-linkage is kept constant for the three-control strategies as observed from Fig. 26. Finally, Fig. 27 shows the input Phase-A current, which would follow the load variation in the three control strategies. Some fluctuation can be observed in the current response for the three control strategies due to some end effect existing in the LIM drive system.

V. Conclusion

In this article, an NSTSM-DTC was proposed for the LIM drive system. The NSTSM algorithm was first employed for both electromagnetic thrust and primary flux linkage control loops. Then the Lyapunov theorem was adopted to analyze the stability of the NSTSM-DTC. The LIM drive performance under the proposed NSTSM-DTC strategy was fully compared with those of the conventional DTC and the CSTSM-DTC methods. Both simulation and experiments have verified that the NSTSM-DTC can get faster dynamic response, stronger robustness, lower thrust chattering in comparison to those of CDTC and CSTSM-DTC. Moreover, the electromagnetic thrust ripple reduction based on the NSTSM-DTC is 7% compared to other two control methods, which can reduce the noises and vibrations effectively in the whole LIM drive system.

References

[1] I. Boldea, L. Tutelea, W. Xu, and M. Pucci, "Linear electric machines, drives and MAGLEVs: An overview," *IEEE Trans. Ind. Electron.*, vol. 65, no. 9, pp. 7504–7515, Sep. 2018.

[2] W. Xu, J. G. Zhu, Y. Wang, Y. Zhang, and L. Tan, "Equivalent circuits for single-sided linear induction motors," *IEEE Trans. Ind. Appl.*, vol. 46, no. 6, pp. 2410–2423, Nov./Dec. 2010.

[3] K. Wang, Y. Li, Q. Ge, and L. Shi, "An improved indirect field-oriented control scheme for linear induction motor traction drives," *IEEE Trans. Ind. Electron.*, vol. 65, no. 12, pp. 9928–9937, Dec. 2018.

[4] J. Lim, J. Jeong, C. Kim, C. Ha, and D. Park, "Analysis and experimental evaluation of normal force of linear induction motor for maglev vehicle," *IEEE Trans. Magn.*, vol. 53, no. 11, Nov. 2017, Art. no. 8300504.

[5] R. Cao, M. Lu, N. Jiang, and M. Cheng, "Comparison between linear induction motor and linear flux-switching permanent-magnet motor for railway transportation," *IEEE Trans. Ind. Electron.*, vol. 66, no. 12, pp. 9394–9405, Dec. 2019.

[6] D. Hu, W. Xu, R. Dian, and Y. Liu, "Loss minimization control strategy for linear induction machine in urban transit considering normal force," *IEEE Trans. Ind. Appl.*, vol. 55, no. 2, pp. 1536–1549, Mar./Apr. 2019.

[7] M. A. M. Cheema, J. E. Fletcher, D. Xiao, and M. F. Rahman, "A direct thrust control scheme for linear permanent magnet synchronous motor based on online duty ratio control," *IEEE Trans. Power Electron.*, vol. 31, no. 6, pp. 4416–4428, Jun. 2016.

[8] Z. Boulghasoul, A. Elbacha, and E. Elwarraki, "Intelligent control for torque ripple minimization in combined vector and direct controls for high performance of IM drive," *J. Elect. Eng. Technol.*, vol. 7, no. 4, pp. 546–557, Jul. 2012.

[9] W. Xu, M. F. Elmorshedy, Y. Liu, J. Rodriguez, and C. Garcia, "Maximum thrust per ampere of linear induction machine based on finite-set model predictive direct thrust control," *IEEE Trans. Power Electron.*, vol. 35, no. 7, pp. 7366–7378, Jul. 2020.

[10] W. Xu, M. M. Ali, M. F. Elmorshedy, S. M. Allam, and C. Mu, "One improved sliding mode dtc for linear induction machines based on linear metro," *IEEE Trans. Power Electron.*, vol. 36, no. 4, pp. 4560–4571, Apr. 2021.

[11] C. Lascu and A. M. Trzynadlowski, "A sensorless hybrid DTC drive for high-volume low-cost applications," *IEEE Trans. Ind. Electron.*, vol. 51, no. 5, pp. 1048–1055, Oct. 2004.

[12] A. A. Naassani, E. Monmasson, and J. P. Louis, "Synthesis of direct torque and flux control by means of sliding-mode theory," *IEEE Trans. Ind. Electron.*, vol. 52, no. 3, pp. 785–799, Jun. 2005.

[13] B. Lu, Y. Fang, and N. Sun, "Continuous sliding mode control strategy for a class of nonlinear underactuated systems," *IEEE Trans. Ind. Electron.*, vol. 63, no. 10, pp. 3471–3478, Oct. 2018.

[14] M. M. Ali, W. Xu, M. F. Elmorshedy, Y. Liu, and M. Dong, "An improved finite-set model predictive current control with nonlinear speed regulator for linear induction machine based on linear metro," in *Proc. IEEE Energy Convers. Congr. Expo.,* 2020, pp. 5141–5147.

[15] W. Xu, A. K. Junejo, Y. Liu, M. G. Hussien, and J. Zhu, "An efficient anti-disturbance sliding-mode speed control method for PMSM drive systems," *IEEE Trans. Power Electron.,* vol. 36, no. 6, pp. 6867–6891, Jun. 2021.

[16] M. M. Ali, W. Xu, M. F. Elmorshedy, Y. Liu, S. M. Allam, and M. Dong, "Sliding mode speed regulation of linear induction motors based on direct thrust control with space-vector modulation strategy," in *Proc. Inter. Conf. Elect. Mach. Syst.*, 2019, pp. 1–6.

[17] A. K. Junejo, W. Xu, C. Mu, M. M. Ismail, and Y. Liu, "Adaptive speed control of PMSM drive system based anew sliding-mode reaching law," *IEEE Trans. Power Electron.,* vol. 35, no. 11, pp. 12110–12121, Nov. 2020.

[18] H. H. Choi, "Sliding-mode output feedback control design," *IEEE Trans. Ind. Electron.*, vol. 55, no. 11, pp. 4047–4054, Nov. 2008.

[19] D. Liang, J. Li, R. Qu, and W. Kong, "Adaptive second-order sliding-mode observer for PMSM sensorless control considering VSI nonlinearity," *IEEE Trans. Power Electron.*, vol. 33, no. 10, pp. 8994–9004, Oct. 2018.

[20] H. Kim, J. Son, and J. Lee, "A high-speed sliding-mode observer for the sensorless speed control of a PMSM," *IEEE Trans. Ind. Electron.,* vol. 58, no. 9, pp. 4069–4077, Dec. 2010.

[21] A. Chalanga, S. Kamal, L. M. Fridman, B. Bandyopadhyay, and J. A. Moreno , "Implementation of super-twisting control: Super twisting and higher order sliding mode observer based approaches," *IEEE Trans. Ind. Electron.*, vol. 63, no. 6, pp. 3677–3685, Jun. 2016.

[22] M. V. Basin and P. C. Rodríguez Ramírez, "A super twisting algorithm for systems of dimension more than one," *IEEE Trans. Ind. Electron.*, vol. 61, no. 11, pp. 6472–6480, Nov. 2014.

[23] B. Tian, J. Cui, H. Lu, L. Liu, and Q. Zong, "Attitude control of UAVS based on event-triggered super twisting algorithm," *IEEE Trans. Ind. Informat.,* vol. 17, no. 2, pp. 1029–1038, Feb. 2021.

[24] B. Brogliato, A. Polyakov, and D. Efimov, "The implicit discretization of the super twisting sliding-mode control algorithm," *IEEE Trans. Autom. Control*, vol. 65, no. 8, pp. 3707–3713, Aug. 2020.

[25] Y. Kali, J. Rodas, M. Saad, R. Gregor, K. Benjelloun, and J. Doval-Gandoy, "Current control based on super-twisting algorithm with time delay estimation for a five-phase induction motor drive," in *Proc. IEEE Int. Elect. Mach. Drives Conf.,* 2017, pp. 1–8.
[26] M. Rasheed *et al.*, "Sensorless second-order sliding-mode speed control of a voltage-feed induction-motor drive using nonlinear state feedback," *IEE Proc Elect. Power Appl.*, vol. 152, no. 5, pp. 1127–1136, Sep. 2005.
[27] L. Zhao, J. Huang, H. Liu, B. Li, and W. Kong, "Second-order sliding-mode observer with online parameter identification for sensorless induction motor drives," *IEEE Trans. Ind. Electron*, vol. 61, no. 10, pp. 5280–5289, Oct. 2014.
[28] C. Lascu, A. Argeseanu, and F. Blaabjerg, "Super twisting sliding-mode direct torque and flux control of induction machine drives," *IEEE Trans. Power Electron*, vol. 35, no. 5, pp. 5057–5065, May 2020.
[29] A. Levant, "Sliding order and sliding accuracy in sliding mode control," *Int. J. Control,* vol. 58, no. 6, pp. 1247–1263, Dec. 1993.
[30] W. Xu, R. Islam, and M. Pucci, *Advanced Linear Machines and Drive Systems*, Berlin, Germany: Springer, Aug. 2019.
[31] R. Seeber, M. Horn, and L. Fridman, "A novel method to estimate the reaching time of the super-twisting algorithm," *IEEE Trans. Autom. Control*, vol. 63, no. 12, pp. 4301–4308, Dec. 2018.

Mosaad M. Ali was born in Kafrelsheikh, Egypt, in 1988. He received the B.Sc. degree from Kafrelsheikh University, Kafr El-Shaikh, Egypt, in 2010, the M.Sc. degree from Alexandria University, Alexandria, Egypt, in 2017, and the Ph.D. degree from the School of Electrical and Electronic Engineering, Huazhong University of Science and Technology, Wuhan, China, in 2021, all in electrical engineering.

He has been a Teaching Assistant with the Department of Electrical Engineering, Faculty of Engineering, Kafrelsheikh University since 2012. In March 2017, he was an Assistant Lecturer. He is currently an Assistant Professor with the Department of Electrical Engineering, Faculty of Engineering, Kafrelsheikh University. His research interests include linear induction motor, sliding mode control, predictive control, and renewable energy.

Wei Xu (Senior Member, IEEE) received the double B.E. and M.E. degrees from Tianjin University, Tianjin, China, in 2002 and 2005, respectively, and the Ph.D. degree from the Institute of Electrical Engineering, Chinese Academy of Sciences, Beijing, China, in 2008, respectively, all in electrical engineering.

From 2008 to 2012, he was a Postdoctoral Fellow with University of Technology Sydney, the Vice Chancellor Research Fellow with Royal Melbourne Institute of Technology, Japan Science Promotion Society Invitation Fellow with Meiji University, respectively. Since 2013, he has been a Full Professor with the State Key Laboratory of Advanced Electromagnetic Engineering, Huazhong University of Science and Technology, Wuhan, China. He has more than 110 papers accepted or published in IEEE Journals, two edited books published by Springer Press, one monograph published by China Machine Press, and more than 150 Invention Patents granted or in pending, all in the related fields of electrical machines and drives. His research topics mainly cover design and control of linear/RMs.

Dr. Xu is a Fellow of the Institute of Engineering and Technology. He served the General Chair for 2021 International Symposium on Linear Drives for Industry Applications in Wuhan, and will serve the General Chair for 2023 IEEE International Conference on Predictive Control of Electrical Drives and Power Electronics in Wuhan. He has been an Associate Editor for several leading IEEE Transactions Journals, such as IEEE TRANSACTIONS ON INDUSTRIAL ELECTRONICS, IEEE TRANSACTIONS ON VEHICULAR TECHNOLOGY, IEEE TRANSACTIONS ON ENERGY CONVERSION, etc.

Abdul Khalique Junejo was born in Larkana, Sindh province, Pakistan, in 1989. He received the bachelor's and master's degrees in electrical engineering from Quaid-e-Awam UEST Nawabshah, Nawabshah, Pakistan, in 2011 and 2015, respectively.

He is currently an Assistant Professor with Quaid-e-Awam UEST Nawabshah. He was a Reviewer for IEEE journals (including IEEE TRANSACTIONS ON INDUSTRIAL ELECTRONICS, IEEE TRANSACTIONS ON POWER ELECTRONICS, IEEE TRANSACTIONS ON TRANSPORTATION ELECTRIFICATION, Emerald Group Publishing Ltd. Assembly Automation, article in Journal and IEEE JOURNAL OF EMERGING AND SELECTED TOPICS IN INDUSTRIAL ELECTRONICS). His research interests include the sliding mode control, direct torque control, model predictive Control and sensorless control methods for permanent magnet synchronous machines, induction machines, and linear IM and drives.

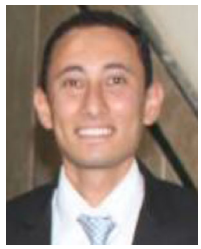

Mahmoud F. Elmorshedy (Member, IEEE) was born in Gharbeya, Egypt, in 1989. He received the B.Sc. and M.Sc. degrees from Tanta University, Tanta, Egypt, in 2012 and 2016, respectively, and the Ph.D. degree from the School of Electrical and Electronic Engineering, Huazhong University of Science and Technology, Wuhan, China, in 2020, all in electrical engineering..

He is currently a Teaching Assistant with the Department of Electrical Power and Machines Engineering, Faculty of Engineering, Tanta University, in 2013. In June 2016, he was an Assistant Lecturer with the Department of Electrical Power and Machines Engineering, Faculty of Engineering, Tanta University. He is currently an Assistant with the Department of Electrical Power and Machines Engineering, Faculty of Engineering, Tanta University. His research interests include linear induction motor, predictive control, power electronics, and renewable energy.

Yirong Tang (Student Member, IEEE) received the B.E. degree in electrical engineering in 2020 from the Huazhong University of Science and Technology, Wuhan, China, where he is currently working toward the Ph.D. degree in electrical engineering with the State Key Laboratory of Advanced Electromagnetic Engineering and Technology.

His research interests include advanced control methods for permanent magnet synchronous machines, linear induction machines and drives.